Wall-modeled large-eddy simulation of a separated flow over the NASA wall-mounted hump

By G. I. Park

1. Motivation

Wall-modeled large-eddy simulation (WMLES) attempts to provide a predictive but affordable framework for LES by modeling the effect of the computationally demanding inner-layer structures on the outer-layer flow. The grids employed in LES are designed to resolve the outer layer only, thereby reducing the computational cost of LES significantly to affordable levels. The saving in the computational cost can easily be a factor of hundreds to thousands for external aerodynamics configurations at flight conditions. Over the past five years, significant improvements to the WMLES technique have been made by the researchers in the Center for Turbulence Research at Stanford University. These include extending the technique to unstructured grid flow solvers (Bodart & Larsson 2011; Park & Moin 2016), identifying and removing some of the error sources in WMLES (Kawai & Larsson 2012), removing ad-hoc tunings in the wall model (Park & Moin 2014), and developing a new class of wall model that is free from the RANS legacy (Bose & Moin 2014). The Center now plans to validate various wall-modeling methods against separating flows over non-trivial geometries using a common computational framework. This is important, because each wall model has been validated independently of other wall models, often against relatively simple flows using different codes. The final goal is applying the state-of-art wall models to realistic three-dimensional configurations relevant to external aerodynamics. This work is a part of the newly embarked NASA-supported project, aimed at increasing the technology-readiness level of WMLES for aerospace applications that is deemed low at this stage.

In this article, we report WMLES of a separated flow over the NASA wall-mounted hump using two standard wall models, as a preliminary work to the aforementioned project. The flow configuration, numerical setup, and wall-modeling approaches are reviewed in Section II. The mean flow predictions from WMLES and the no-slip LES calculation are presented in Section III with comparison to the experimental measurements. The importance of resolving the thin, attached shear layer in the pre-separation region will be highlighted, with an emphasis on local mesh adaptations.

2. Computational details

2.1. *Flow configuration*

The flow configuration considered in the present study is the separated flow over the NASA wall-mounted hump. The experiment of Greenblatt *et al.* (2006) with no flow control is used here as reference. This configuration is well-documented under the Turbulence Modeling Resource website administered by the NASA Langley Research Center (http://turbmodels.larc.nasa.gov/). This case was considered as a benchmark case for evaluating a variety of RANS methods in the 2004 CFD Validation Workshop (Rumsey *et al.* 2006), and it was subsequently studied with LES in a few studies (You *et al.* 2006;

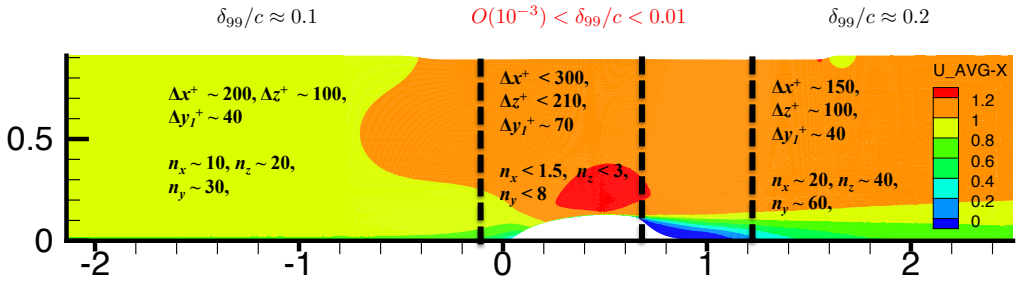

FIGURE 1. Computational domain with mesh and boundary layer thickness (δ/c) information. n_x, n_y, and n_z are the number of boundary-layer-thickness resolving cells in the streamwise, wall-normal, and spanwise directions, respectively. Δx^+ and Δz^+ are the grid spacings in the x and z directions, respectively. Δy_1^+ is the the wall normal grid spacing of the wall-adjacent cells (i.e., twice the distance between the cell center and the wall). The background color contour is for the mean streamwise velocity nomalized with the inlet freestresm velocity (U/U_∞).

Avdis *et al.* 2009). The hump geometry is a Glauert-Goldschmied type body mounted on the wall. It has a long fore-body along which the incident boundary layer grows under a favorable pressure gradient, followed by a relatively short and concave aft-body on which the boundary layers separates. The flow expands rapidly and separates around the apex of the hump, experiencing a strong adverse pressure gradient. Compared to the the smooth body separations caused by a gradual development of the adverse pressure gradient (e.g., airfoils and diffusers at near-stall conditions), the flow separation on the hump is forced by the geometry. A challenge in CFD analyses has been to predict the boundary layer reattachment and its recovery to the equilibrium state.

The computational domain is of size $L_x \times L_y \times L_z = 4.64c \times 0.909c \times 0.3c$, where c is the hump chord length. Here, x, y, and z denote the streamwise, wall-normal, and spanwise directions, respectively (see figure 1). The origin of the simulation coordinate is located on the leading edge of the hump. The inlet and the outlet of the computational domain are located at $x/c = -2.14$ and $x/c = 2.5$, respectively. The top-wall boundary is located nominally at $y/c = 0.909$, with a slight constriction between $x/c \approx -0.5$ and $x/c \approx 1.6$ to account for the blockage effect due to the side plates in the experiment (see Rumsey *et al.* (2006) for details). This modification of the top-wall geometry was adopted in most of the reported RANS and LES calculations (You *et al.* 2006; Avdis *et al.* 2009; Rumsey *et al.* 2006). The spanwise domain size is $L_z = 0.3c$, which is in between the size considered in the two past LES studies ($L_z = 0.2c$ in You *et al.* (2006) and $L_z = 0.4c$ in Avdis *et al.* (2009)). The present spanwise box size is chosen based on the observation of You *et al.* (2006). They showed that the pressure coefficients predicted with $L_z = 0.15c$ and $L_z = 0.2c$ had little difference.

The freestream Mach number is kept at $M = 0.2$ in all simulations. Although this is slightly higher than the Mach number in the experiment ($M = 0.12$), we expect this has negligible effect in the mean flow, based on our prior experience of comparing low Mach simulations to the incompressible references (Park & Moin 2014; Balakumar *et al.* 2014). The Reynolds number based on the hump chord c, the inlet freestream velocity U_∞, and the kinematic viscosity ν is $Re_c = U_\infty c/\nu = 935,892$. The experiment report the mean velocity and the streamwise intensity at $x/c = -2.14$ upstream of the hump for

prescription of the inflow condition in CFD. At this location, the momentum-thickness Reynolds number (Re_θ) computed with the WMLES solution was about 8,000, and it increased beyond 10^4 by the time flow reached the leading edge of the hump. Herein, the momentum-thickness Reynolds number is defined with $Re_\theta = U_\infty\theta/\nu$, where θ is the integral momentum thickness. θ was computed from a velocity profile composed of the wall-model solution and the LES solution above the matching location. Although the chord Reynolds number (Re_c) alone may be considered low for introducing near-wall models, the high Reynolds number nature of the incident boundary layer necessitates wall modeling for its adequate representation on the coarse grids employed in the present study.

In the baseline LES grid shown in Figure 2 (hereinafter referred as G1), the number of cells in the streamwise and the wall-normal directions are $N_x = 1238$ and $N_y = 110$, respectively. The grid is nested in the spanwise direction to fully leverage the flexibility of the unstructured grid solver. At $y/c > 0.3$ in which no complex flow structures exist, the number of cells in the spanwise direction is kept low at $N_z = 20$. The meshes below $y/c = 0.3$ are refined in two level using a grid adaptation tool *adapt*† to have $N_z = 80$. The number of cells in the grid G1 then totals 5.9 million. Figure 3 characterizes the grid resolution in terms of the viscous wall units. The grid G1 is very coarse, having $\Delta x^+ \geq 200$, $\Delta z^+ \geq 100$, and $\Delta y_1^+ \geq 40$ in the most attached region. A metric that is more relevant in characterizing the grid resolution in WMLES is the near-wall cell density per δ (boundary layer thickness) in each direction. The standards for this density suggested in the literature fall in the range of 10∼30 (Choi & Moin 2012; Chapman 1979). The grid G1 satisfies this condition well in the attached region outside the hump. However, the cell density is extremely low (especially in the wall-parallel directions) in the attached region on the hump, owing to the very thin boundary layer developing there (see Figure 1). Especially, the boundary layer on the first one-third of the hump is barely resolved, having less than three cells in the wall-normal direction across the shear layer. In order to examine the effect of not properly resolving the thin attached shear layer, a grid G2 obtained from G1 by refining the first 4 layers of the wall-adjacent cells in the range of $-0.5 \leq x/c \leq 1.6$ twice in the wall-normal direction is also considered. The number of cells in the grid G2 increases by 8% compared to G1, totaling 6.4 million. Table 1 compares the domain size and the number of grid points in the present and the past computational studies. The number of grid points in the table pertain only to the main hump simulation. If the cost related to the inflow generation was considered together, the present WMLES would be at least 2∼4 times cheaper than the LES/WMLES studies of You *et al.* (2006) and Avdis *et al.* (2009). In the present study, the inflow data are generated without requiring a companion recycle simulation (Lund *et al.* 1998), and therefore the the cost of inflow generation is negligible (see Sec. II 2.2).

2.2. *Boundary conditions*

The symmetry condition is imposed on the top-wall boundary. The subsonic-outlet Navier-Stokes Characteristic Boundary Condition (NSCBC) (Poinsot & Lele 1992) is applied at the outlet. Periodic boundary conditions are used along the spanwise direction. The wall-stresses obtained from the wall model are applied on the bottom wall as Neumann Boundary conditions. The wall is assumed to be thermally adiabatic.

At the inflow plane located at $x/c = -2.14$, synthetic signals constructed with a digital filtering technique (Klein *et al.* 2003) are imposed to provide turbulent inflow data that

† Cascade Technologies, Inc.

Authors (type)	number of cells (main simulation)	Inflow generation	x-domain size (L_x/c) (main/inflow)	z-domain size (L_z/c)
Present (WMLES)	**5.9M**	**Synthetic turbulence**	**4.64/0**	**0.3**
You *et al.* (LES)	7.5M	Recycle	4.5/not reported	0.2
Avdis *et al.* (WMLES)	9.4M	Recycle	2.81/2.14	0.4

TABLE 1. Principal parameters of the present and past simulation studies. For LES with the NEQWM, the number of cells is 5.9M (LES) + 2M (WM) = 7.9M including the wall-model grid. Two numbers is the x-domain size are the streamwise domain size of the main hump simulation and the inflow-recycle simulation (if any), respectively.

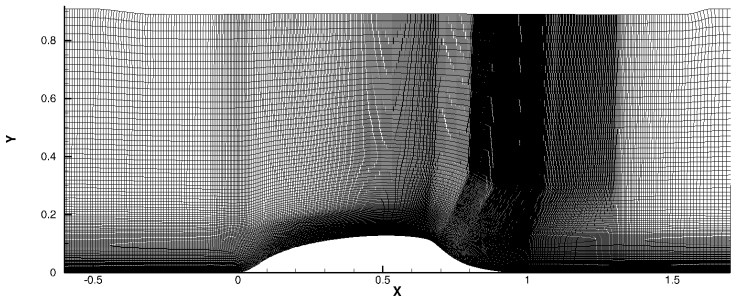

FIGURE 2. Computational mesh in the x-y plane from the grid G1 in the vicinity of the hump geometry.

match the experiment. This technique generates a sequence of random fluctuating signals that matches the user-provided mean and covariance (the Reynolds stresses). Since only the mean and the streamwise intensity are available from the experiment, the missing Reynolds stress components were specified somewhat arbitrarily by scaling the data from a boundary layer LES (Schlatter *et al.* 2010) at a lower Reynolds number. The left panels in Figure 4 show that the mean velocity at the inflow plane matches the experiment very well, and that the agreement of the streamwise intensity is acceptable. The right panels in Figure 4 compare the mean velocity and the Reynolds stresses from the present WMLES at a downstream location ($x/c = -0.81$) to the data from WMLES of Avdis *et al.* (2009). Excellent agreement is observed. This assures that the inflow has evolved from random signals to realistic turbulence well before reaching the hump.

2.3. *Wall modeling and flow solver*

In the present study, two standard wall models in the category of wall-flux models are considered: non-equilibrium wall model and equilibrium wall model. In these approaches, simplified or full Navier-Stokes equations are solved on a separate near-wall domain. The wall models are driven by the LES data superimposed on the top boundaries of the wall model. At each time step, the wall-shear stress (τ_w) and the wall-heat flux (q_w) required to advance the very coarse LES are obtained directly from the wall-model solution (see Figure 5). The wall-model grid usually has the same wall-parallel mesh content as that of

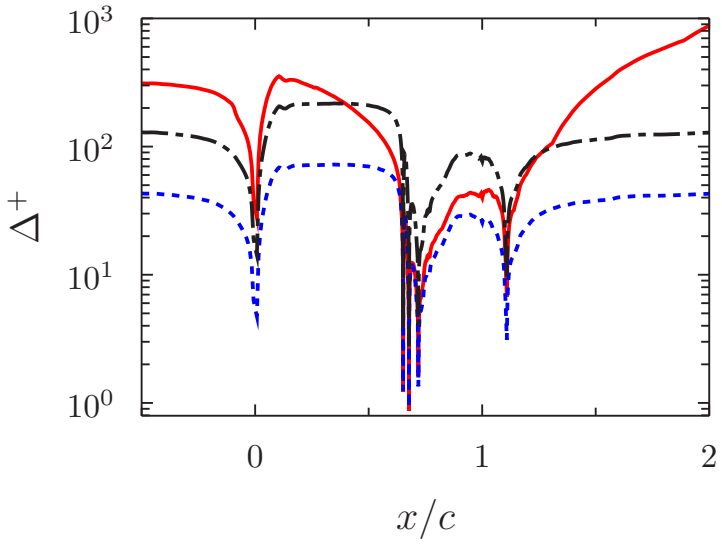

FIGURE 3. Grid spacings in wall unit ($\Delta^+ \equiv u_\tau \Delta/\nu$, where $u_\tau^2 = \tau_w/\rho$) in the baseline grid G1. Red solid line, Δx^+ (tangential grid spacing); black dash-dotted line, Δz^+ (spanwise grid spacing); blue dotted line, Δy_1^+ (wall-normal grid spacing). The friction velocity (u_τ) is based on the local wall-shear stress (τ_w). The hump geometry spans the range $0 \leq x/c \leq 1$.

the primal LES grid. However, the wall-model grid must have significantly finer resolution in the wall-normal direction to impose the no-slip wall condition directly.

The wall models have been implemented in the code *Charles*†, an unstructured grid finite volume compressible LES solver. The code solves the low-pass filtered compressible Navier-Stokes equations with the dynamic Smagorinsky model (Moin *et al.* 1991; Lilly 1992) for the subgrid-scale (SGS) closure. The code uses a low-dissipation second-order spatial discretization with an explicit RK3 scheme for time integration. Details of the code can be found in Park & Moin (2016) and Park (2014). Applications of the combined WMLES solver to single- and multi-element airfoils as well as canonical wall-bounded flows are reported in separate publications (Park & Moin 2014; Bodart & Larsson 2011; Balakumar *et al.* 2014).

The non-equilibrium wall model (hereinafter, the "NEQWM") solves the unsteady 3-D Navier-Stokes equations with a RANS-type turbulence closure (Park & Moin 2014, 2016). Like the primal LES solver, the NEQWM itself is a full flow solver requiring a regular, connected grid. In the present study, the wall-model grid consists of 2 million cells. It is constructed from the primal LES grid by retaining only the first 4 layers of the wall-adjacent cells, and subsequently refining these cells only in the wall-normal direction. The wall-model grid has the same mesh content in the wall-parallel directions as that of the LES grid, but it has 30 cells stretched in the wall-normal direction to resolve the viscous sublayer. To avoid the severe acoustic CFL restriction on the time step caused by the small near-wall normal grid spacing, a fully implicit time integration is used in the NEQWM.

The equilibrium wall model (hereinafter, the "EQWM") is derived from the NEQWM by neglecting all the terms except for the wall-normal diffusion (Bodart & Larsson 2011).

† Cascade Technologies, Inc

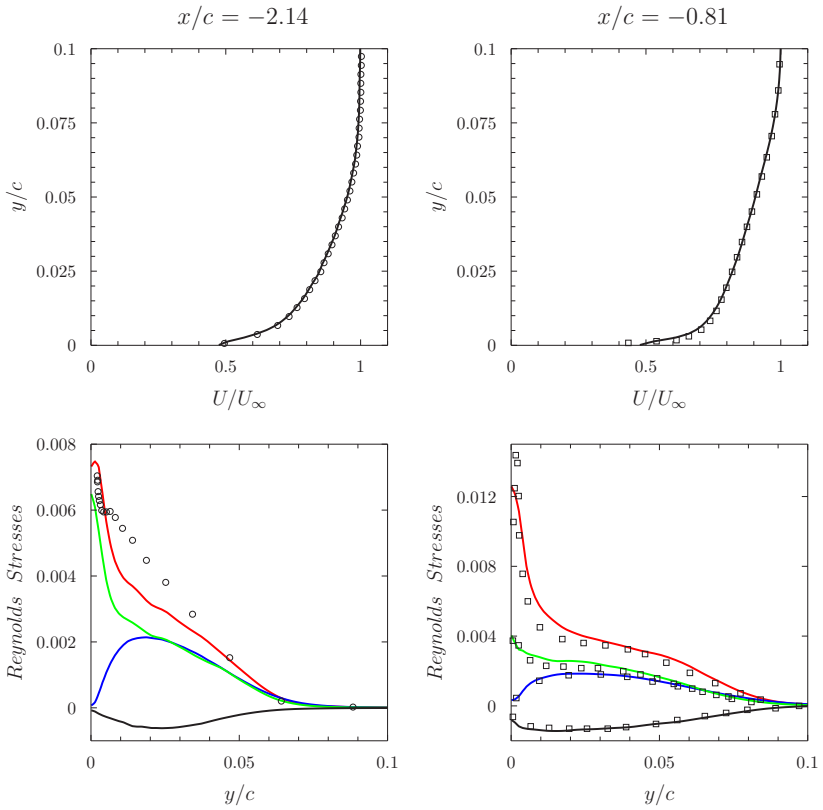

FIGURE 4. The mean streamwise velocity and the Reynolds stresses at the inflow plane ($x/c = -2.14$) and a downstream location ($x/c = -0.81$). Red lines, $\overline{u'^2}$; green lines, $\overline{w'^2}$; blue lines, $\overline{v'^2}$; black lines (bottom panels), $\overline{u'v'}$; circles (left panels), experiment (Greenblatt *et al.* 2006); squares (right pannels), WMLES (Avdis *et al.* 2009)

The EQWM reduces to a system of two coupled ordinary differential equations that is solved along the wall-normal direction on each wall face. No regular grid is required, and the wall-normal grid can be defined implicitly along the normal vector. In the present study, the wall-normal grid in the EQWM has 30 cells, same as the NEQWM. Additionally, the matching location (or the wall-model layer thickness) is kept the same as that of the NEQWM.

The location at which the wall model receives the LES data (matching location) is an implicit modeling parameter in all wall-flux models. It is generally agreed on that WMLES solution of attached flows is insensitive to the matching location, provided that it is placed within the logarithmic layer of the mean velocity profile, and that at least three cells are placed below the matching location (Kawai & Larsson 2012, 2013; Park & Moin 2014). No general rule is available for the matching location in separated flows, but it is suggested to place the matching location well beneath the recirculation zone so that the wall model see mostly unidirectional flows along the wall-normal direction (Park & Moin 2016). This is partly because the turbulence models employed in the wall models often fail to reproduce the dynamics of the recirculating flow as a whole. Instead, the more accurate LES resolves most of the separated region directly, while the wall model

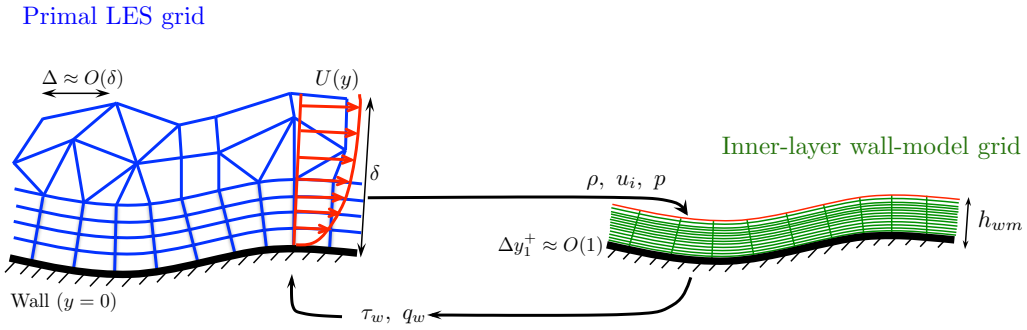

FIGURE 5. Illustration of the wall-flux modeling presented in Park & Moin (2016).

is driven passively by the LES data. This would be particularly pertinent to the EQWM, which by construction cannot represent the sign change in the velocity gradient.

2.4. *Cost of wall modeling*

All simulations in the present study were carried out with 512 cores on the Pinto cluster, a modest-sized high-performance computing platform operated by Los Alamos National Laboratory (LANL). The cluster has 2464 CPU cores (Intel Xeon E5-2670 2.6 GHz) on 154 compute nodes (16 cores/node), with 32 GB/node memory and Qlogic InfiniBand Fat-Tree interconnect. All calculations took less than 40 wall-clock hours to advance 20 flow-through times (c/U_∞). The average wall-clock time spent for integrating 10 simulations time steps were 1.6s, 2.2s, and 3.3s for the no-slip LES (no wall model), the LES with the EQWM, and the LES with the NEQWM, respectively. Extra costs of wall modeling for the EQWM and the NEQWM are therefore about 40% and 100% of the stand-alone LES, respectively. The higher cost of the NEQWM is due to the matrix inversion associated with the fully implicit time integration. In general, the cost of wall modeling is a substantial fraction of the stand-alone LES. However, this should be deemed affordable, because the grids employed in WMLES of high Reynolds number flows are already significantly coarser than the grids used for wall-resolved LES.

3. Results

Figure 6 compares the mean streamwise velocity profiles obtained with the grid G1 to the experiment. Various streamwise locations from near the apex of the hump to the downstream of the reattachment point are considered (the flow reattaches at $x/c = 1.1$ in the experiment). It is obvious that the no-slip LES fails on the grid G1. In the no-slip LES, the boundary layer on the hump carries too high momentum due to the significantly under-predicted wall-shear stress. Consequently, the separation bubble is too small and the flow reattaches too early. The velocity profiles after the reattachment are also grossly mispredicted with too high momenta. With wall modeling, prediction of the mean velocity improves dramatically. In WMLES, the velocity profiles immediately prior to the separation at $x/c = 0.65$ are in close agreement with the experiment, implying that the attached flow on the hump is reproduced well with correct momentum. The profiles in the separated and post-reattachment regions are in reasonable agreement with

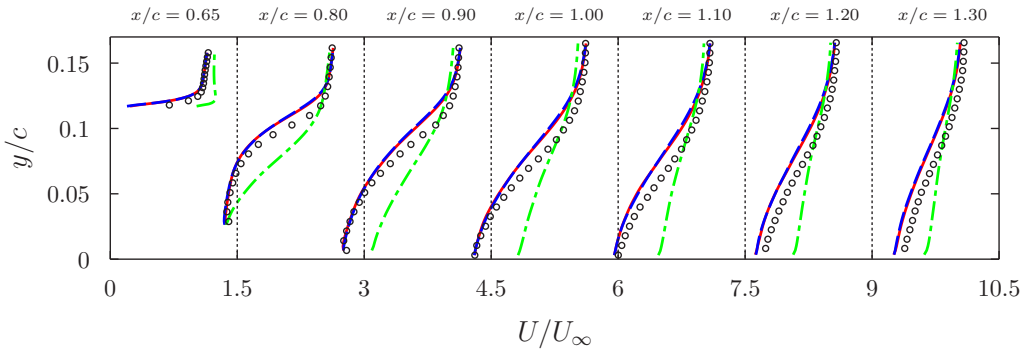

FIGURE 6. The mean streamwise velocity from simulations with the grid G1. Red solid line, LES with the NEQWM; blue dashed line, LES with the EQWM; green dashed-dotted line, no-slip LES; circles, experiment (Greenblatt *et al.* 2006). Profiles are shifted by 1.5, 3, $\cdots$, 9 along the abscissa.

the measurement. Although the skin friction data have not been post-processed yet, it can be deduced from the velocity profiles that the flow reattaches very close to $x/c = 1.1$ as in the experiment. Slight momentum deficits are observed in the profiles downstream of $x/c = 0.8$, which we suspect to be caused by the insufficient grid resolution in the thin shear layers on the hump fore-body, and in the outer layers. Additionally, it is noteworthy that predictions with two different wall models are nearly indistinguishable at this grid resolution. Similar observations are made on the Reynolds stress profiles (Figure 7). Prediction improves significantly with wall modeling, especially in the separated region.

Figure 8 shows the mean pressure coefficients ($-C_p$) along the bottom wall. In the no-slip LES, the pressure minimum on the hump apex is significantly under-predicted due to the over-accelerated flow. The plateau characterizing the separation in $0.7 < x/c < 0.9$ is missing in the no-slip LES. The pressure coefficients from WMLES are in reasonable agreement with the experiment.

Figures 9 and 10 show the predictions of the mean velocity and the pressure coefficient with the grid G2. Recall that the grid G2 is identical to the grid G1, except that the grid G2 has four times finer resolution in the normal direction below the matching location. This increases the number of boundary-layer-resolving cells in the normal direction from about 2$\sim$3 to 8$\sim$12 for the thin attached shear layer on the hump fore-body. With the grid G2, a noticeable improvement in the prediction of the outer layer profiles is observed. Note that the results from the no-slip LES are also improved significantly with the grid G2, although the separation is still too weak. Similar observations are made on the pressure coefficients. C_p from the no-slip LES is now in reasonable agreement with the experiment, but the WMLES results show excellent collapses with the experiment. Overall, this observation suggests that having a reasonable resolution in the thin, incident shear layer is important in capturing the separation. In the present study, this was achieved by exploiting a local adaptation technique, accompanying only 10% increase in the total cell count.

4. Conclusion

Large-eddy simulations with two wall modeling techniques have been applied to a separated flow over the NASA wall-mounted hump. It was shown that LES with the equi-

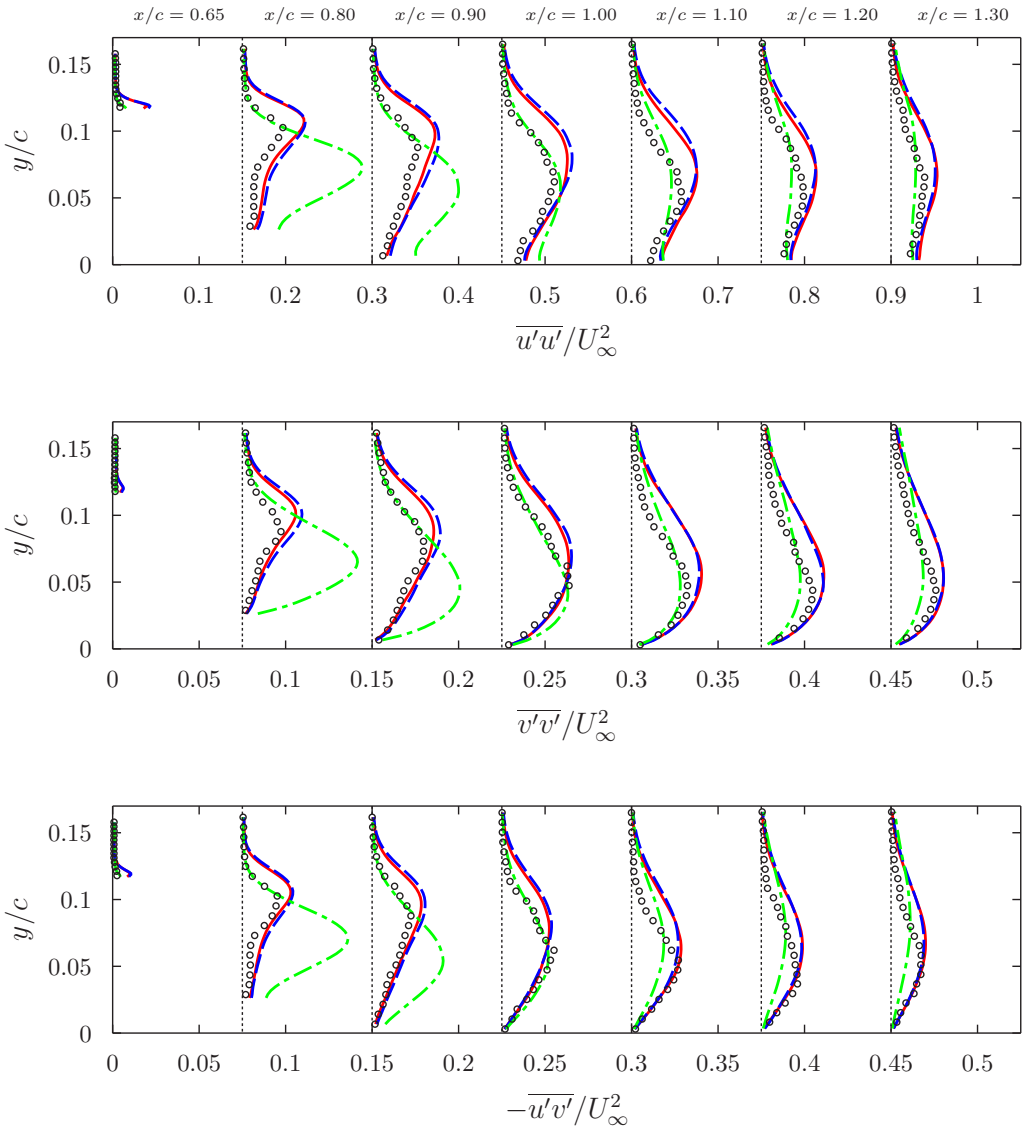

FIGURE 7. Profiles of the resolved Reynolds stresses from simulations with the grid G1. Red solid line, LES with the NEQWM; blue dashed line, LES with the EQWM; green dashed-dotted line, no-slip LES; circles, experiment (Greenblatt *et al.* 2006). Profiles of $\overline{u'u'}$ are shifted by 0.15, 0.3, $\cdots$, 0.9 along the abscissa. Profiles of $\overline{v'v'}$ and $-\overline{u'v'}$are shifted by 0.075, 0.15, $\cdots$, 0.45 along the abscissa.

librium wall model and the non-equilibrium wall model predict the mean flow field accurately on a coarse grid where the no-slip LES catastrophically fails. It was demonstrated that properly resolving the thin attached shear layer developing on the pre-separation region improves the mean flow prediction. This was done by using a local mesh adaptation utility (*adapt* of Cascade Technologies, Inc.) well-suited for unstructured grid solvers with less than 10% increase in the total cell count. Calculations with different wall models

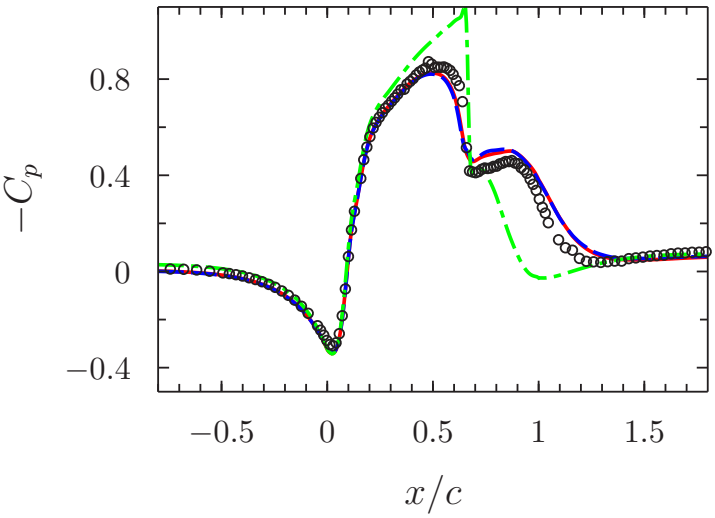

FIGURE 8. Pressure distribution along the bottom wall from simulations with the grid G1. Red solid line, LES with the NEQWM; blue dashed line, LES with the EQWM; green dashed-dotted line, no-slip LES; circles, experiment (Greenblatt *et al.* 2006).

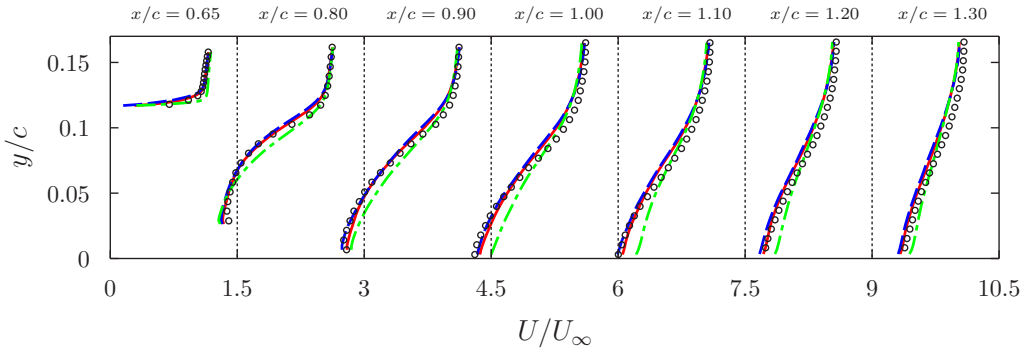

FIGURE 9. The mean streamwise velocity from simulations with the grid G2. Red solid line, LES with the NEQWM; blue dashed line, LES with the EQWM; green dashed-dotted line, no-slip LES; circles, experiment (Greenblatt *et al.* 2006). Profiles are shifted by 1.5, 3, $\cdots$, 9 along the abscissa.

produced nearly identical results. It is suspected that the difference in the model performance, albeit expected to be modest, would be more pronounced in flows where history effects are important and the non-equilibrium effects are global. (e.g., stalled diffuser, massive separation on airfoils). Application of WMLES to such separating flows with various wall models is currently planned for the upcoming years.

Acknowledgments

This work was supported by the the NASA under the Subsonic Fixed-Wing Program (Grant NNX11AI60A) and the Transformative Aeronautics Concepts Program (Grant NNX15AU93A).

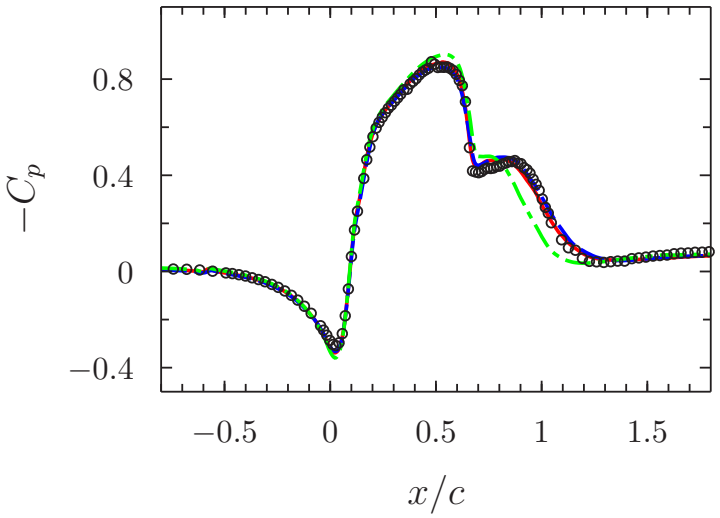

FIGURE 10. Pressure distribution along the bottom wall from simulations with the grid G2. Red solid line, LES with the NEQWM; blue dashed line, LES with the EQWM; green dashed-dotted line, no-slip LES; circles, experiment (Greenblatt *et al.* 2006).

REFERENCES

AVDIS, A., LARDEAU, S. & LESCHZINER, M. 2009 Large eddy simulation of separated flow over a two-dimensional hump with and without control by means of a synthetic slot-jet. *Flow Turb. Combust.* **83**, 343–370.

BALAKUMAR, P., PARK, G. I. & PIERCE, B. 2014 DNS, LES, and wall-modeled LES of separating flow over periodic hills. *Proceedings of the Summer Program*, Center for Turbulence Research, Stanford University, pp. 407–415.

BODART, J. & LARSSON, J. 2011 Wall-modeled large eddy simulation in complex geometries with application to high-lift devices. *Annual Research Briefs*, Center for Turbulence Research, Stanford University, pp. 37–48.

BOSE, S. T. & MOIN, P. 2014 A dynamic slip boundary condition for wall-modeled large-eddy simulation. *Phys. Fluids* **26**, 015104.

CHAPMAN, D. R. 1979 Computational aerodynamics development and outlook. *AIAA J.* **17**, 1293.

CHOI, H. & MOIN, P. 2012 Grid-point requirements for large eddy simulation: Chapman's estimates revisited. *Phys. Fluids* **24**, 011702.

GREENBLATT, D., PASCHAL, K. B., YAO, C. S., HARRIS, J., SCHAEFFLER, N. W. & WASHBURN, A. E. 2006 A separation control CFD validation test case part 1: Baseline and steady suction. AIAA Paper 2004-2220, June 2004.

KAWAI, S. & LARSSON, J. 2012 Wall-modeling in large eddy simulation: length scales, grid resolution, and accuracy. *Phys. Fluids* **24**, 015015.

KAWAI, S. & LARSSON, J. 2013 Dynamic non-equilibrium wall-modeling for large eddy simulation at high Reynolds numbers. *Phys. Fluids* **25**, 015105.

KLEIN, M., SADIKI, A. & JANICKA, J. 2003 A digital filter based generation of inflow data for spatially developing direct numerical or large eddy simulations. *J. Comput. Phys.* **186**, 652–665.

Lilly, D. K. 1992 A proposed modification of the Germano subgrid-scale closure method. *Phys. Fluids* **4**, 633–635.

Lund, T. S., Wu, X. & Squires, K. D. 1998 Generation of turbulent inflow data for spatially- developing boundary layer simulations. *J. Comput. Phys.* **140**, 233–258.

Moin, P., Squires, K., Cabot, W. & Lee, S. 1991 A dynamic subgrid-scale model for compressible turbulence and scalar transport. *Phys. Fluids* **3**, 2746.

Park, G. I. 2014 Wall-modeled large eddy simulation in an unstructured mesh environment. PhD dissertation, Stanford University, Stanford, CA, US.

Park, G. I. & Moin, P. 2014 An improved dynamic non-equilibrium wall-model for large eddy simulation. *Phys. Fluids* **26**, 015108.

Park, G. I. & Moin, P. 2016 Numerical aspects and implementation of a two-layer zonal wall model for LES of compressible turbulent flows on unstructured meshes. *J. Comput. Phys.* **305**, 589–603.

Poinsot, T. J. & Lele, S. K. 1992 Boundary conditions for direct simulations of compressible viscous flows. *J. Comput. Phys.* **101**, 104–129.

Rumsey, C. L., Gatski, T. B., III, W. L. S., Vasta, V. N. & Viken, A. 2006 Summary of the 2004 computational fluid dynamics validation workshop on synthetic jets. *AIAA J.* **44** (2), 194–207.

Schlatter, P., Li, Q., Brethouwer, G., Johansson, A. V. & Henningson, D. S. 2010 Simulations of spatially evolving turbulent boundary layers up to $Re_\theta = 4300$. *Int. J. Heat Fluid Flow* **31**, 251–261.

You, D., Wang, M. & Moin, P. 2006 Large-eddy simulation of flow over a wall-mounted hump with separation control. *AIAA J.* **44** (11), 2571–2577.